An electrochemical treatment to improve corrosion and contact resistance of stainless steel bipolar plates used in polymer electrolyte fuel cells

CrossMark

Ebrahim M. Gabreab [a], Gareth Hinds [b,*,1], Sarah Fearn [c], David Hodgson [a], Jason Millichamp [a], Paul R. Shearing [a], Daniel J.L. Brett [a,*,1]

[a] Electrochemical Innovation Lab, Department of Chemical Engineering, UCL, London WC1E 7JE, UK
[b] National Physical Laboratory, Hampton Road, Teddington, Middlesex TW11 0LW, UK
[c] Department of Materials, Imperial College London, South Kensington Campus, Exhibition Road, London SW7 2AZ, UK

HIGHLIGHTS

- Treatment for improving corrosion/contact resistance of stainless steel bipolar plates.
- Contact resistance of 316 stainless steel is reduced by over 800% at 140 N cm^{-2}.
- Treatment found to enhance Cr concentration in the near-surface.

ARTICLE INFO

ABSTRACT

An electrochemical surface treatment is presented that improves the properties of stainless steel (316SS) used as bipolar plates for polymer electrolyte fuel cells (PEFCs). The process is an anodic treatment, whereby the material is polarised beyond the transpassive region. Potentiodynamic corrosion testing, chemical and morphological surface characterisation and interfacial contact resistance measurements indicate that the improved properties of 316SS are primarily a consequence of an enrichment of Cr at the near-surface of the material. The surface treatment increases the corrosion resistance and significantly reduces interfacial contact resistance.

© 2013 Elsevier B.V. All rights reserved.

1. Introduction

The polymer electrolyte fuel cell (PEFC) has shown great promise as a power source for stationary and transportation applications, largely due to its high power density and low temperature (typically 60–80 °C) operation. Although great strides have been made in the development of the various components for the PEFC, factors such as material performance, durability and production costs continue to retard development of fuel cells. The bipolar plate is an example of a component that still requires significant improvement in order to optimise performance and realize operating targets [1].

The bipolar plate must carry fuel and oxidant to the respective electrodes and disperse the fluid in an even and controlled manner, it must conduct electronic current from each electrode, provide mechanical support and strength to the membrane electrode assembly (MEA), remove excess product water from the reaction zone, help control the temperature of the fuel cell by acting as a heat sink and physically separate reactant streams.

The cost of bipolar plate materials and processing required during manufacture make it one of the most expensive parts of the fuel cell. The bipolar plate typically accounts for 80–85% of the weight and most of the volume of fuel cell stacks [2]. Hence, low cost and lightweight materials are needed which do not compromise performance and durability.

* Corresponding authors. Tel.: +44 (0)20 7679 3310.
 E-mail address: d.brett@ucl.ac.uk (D.J.L. Brett).
[1] URL: http://www.ucl.ac.uk/centre-for-co2-technology

The multiple roles of the bipolar plate and the challenging environment in which it operates mean that the ideal material should be able to operate in an acidic environment (pH 3–5) in the presence of F^- ions (leached from the electrolyte membrane – particularly during start-up), potentials of 0–1.6 V vs. RHE (reversible hydrogen electrode) [3] and a temperature range of 60–120 °C [4]. The ideal bipolar plate should incorporate excellent corrosion properties, resistance to ion leaching, minimum electrical resistivity, be chemically and thermally stable as well as have good thermal conductivity, high mechanical strength and have a low contact resistance with the gas diffusion layer (GDL). Furthermore, they need to be thin and lightweight to increase the volumetric and gravimetric power density, be inexpensive and easy to fabricate as well as being environmentally benign in terms of manufacture and ultimate disposal/recycling.

Due to the need to maximise the power densities of PEFCs and lower the cost of construction, metallic bipolar plates are a popular choice for this component, albeit with the challenge of corrosion. Among many candidate materials based on metals and alloys, stainless steel has attracted much attention [5]. The advantages of using stainless steel are low cost, high strength and ease of incorporating a flow field via stamping or embossing. However, stainless steels are prone to chemical attack in the PEFC environment and corrosion products may poison the catalysts and/or ionomer membrane [6], which can have a significant effect on PEFC stack efficiency and cost [7].

In order to overcome the shortcomings of stainless steel with regards to corrosion, various surface coating and modification techniques have been proposed, including chemical vapour deposition (CVD) [8], physical vapour deposition (PVD) [9], electroplating [10] and nitriding [11]. It has also been reported that Cr-enriched surfaces can be beneficial to the interfacial contact resistance (ICR) [12].

The performance of stainless steel is limited by its surface characteristics, one of the issues being the voltage drop at the interface with the GDL due to the contact resistance associated with insulating surface oxides [1]. The nature of the surface oxide is a function of the alloying elements and the environment in which it operates inside the fuel cell. Studies by Davies et al. identified 316, 310 and 904L as promising grades of stainless steel based on the contact resistance and polarization characteristics [13]. It was noted that an increased Ni and Cr content in the alloy leads to lower interfacial resistance due to the formation of a thinner passive film. Wang et al. also investigated the applicability of different austenitic stainless steel compositions for bipolar plates by simulating the chemical environment of PEFCs [5]. Similarly it was concluded that decreasing contact resistance and corrosion current were observed for steels with increasing Cr content. The performance generally increases in the order 349TM > 904L > 317L > 316L. The results of these studies confirmed that Cr content plays a very important role in reducing ICR and consequently improves the performance of PEFCs.

Electrochemical processes resulting in chromium surface enrichment have been reported under traditional electropolishing conditions [14–16], as well as improving the passivity of iron-chromium alloys in dilute acid conditions [17]. Lee et al. developed an electrochemical process to increase the Cr activity at the surface of stainless steel to obtain a corrosion-resistant oxide [18]. Kim et al. demonstrated using specimens that underwent surface modification by immersion in acidic solution followed by heat treatment that rougher surfaces showed a lower ICR [19].

Electropolishing involves the dissolution of metal from the surface to produce a uniquely advantageous surface finish compared to the cutting, tearing and smearing action of abrasives and cutting tools which deforms the near-surface material, generating significant levels of residual stress. It may be used in lieu of abrasive fine polishing in microstructure preparation [20]. Electropolishing is an effective means of passivating stainless steel, for example electropolished steel parts have been stored at 60–70% relative humidity for six months without visible rust [21]. It is a method for achieving new surface qualities that are outstanding in many applications while ensuring cost saving and technical improvements are realised. In addition to the decrease in the corrosion current density due to the formation of a passive surface film enriched with chromium, greater heat reflectivity and better emissivity may also be achieved [14].

Electropolishing is normally carried out in concentrated acid media and the polishing process is thought to involve the formation of a viscous layer at the metal surface, which can be enhanced by employing viscosity modifiers such as glycerol [14,20,21]. While electropolishing is a well-established industrial process there are issues associated with the technology, most notably that the solution used is highly corrosive and toxic, with extensive gas evolution occurring during the process.

Electropolishing is generally classified into two processes, surface levelling/roughening (etching) and surface brightening [22,23]. Electroetching is the process of surface roughening, with a matt finish result characterised by shallow pitting [15]. Etching is commonly performed on stainless steel (e.g. 0.05 A cm^{-2} in 0.5 M Na_2SO_4 under alkaline conditions) [24]. Brightening is commonly carried out in co-acidic electrolytes of H_2SO_4 and H_3PO_4, with glycerol commonly used as an additive to suppress the influence of the metal microstructure on the dissolution rate [23].

Voltage transients under galvanic control can be used as an indicator of whether etching or brightening is taking place during anodisation treatments. At low current densities, when the dissolution voltage remains constant, the whole electrode is etched, while the formation of peaks at higher current densities usually corresponds to brightening [25].

The main objectives of the electropolishing process are: firstly, to remove the solid (Beilby) layer that consists of inclusions of martensitic phase, foreign material, and pre-existing oxides created by forming, machining or abrasive polishing [14,26]. Secondly, to create a new corrosion resistant layer that is enriched in chromium oxide due to anomalous co-dissolution and thirdly, to equipotentialize the grain boundaries of metallic materials [16].

While the electropolishing process is generally performed in quiescent electrolytes, flow dependent current plateaus that accompany electropolishing are observed [14,27]. The use of high current densities is also typically associated with the process. Although a low current is desirable in order to ensure a high current efficiency, consequently reducing hydrogen evolution and the flammability hazard [25], use of dilute electrolytes would help reduce this risk.

Sulphate-containing electrolytes are preferred for stainless steel dissolution as many reducing agents, which produce sulphate anions, are available to convert Cr^{6+} to Cr^{3+} [15]. Furthermore, the use of dilute sulphate electrolytes at low current densities has been shown to bring about improved surface qualities [25].

The rate determining process during electropolishing is diffusion of product ions away from the surface. The properties of this diffusion layer are affected by its viscosity, which can be used as a means of controlling the process. The viscosity of the polishing film may be modified by addition of a viscosity enhancing agent, typically a polyol, e.g. glycerol (propane-1,2,3-triol). On this basis, the preferential dissolution of ions from microscopic protrusions on the surface of the metal can be accounted for by the difference in the concentration gradient over the 'peaks', where the diffusion layer is thin and the concentration gradient is high, and 'valleys' where the diffusion layer is thicker and concentration gradient is lower.

This paper describes an electrochemical process applied to 316SS that is capable of improving the corrosion properties and electrical contact resistance with gas diffusion electrodes, with a view to use as bipolar plates in PEFCs. The effect of electrolyte concentration, treatment time and the addition of a viscosity modifier are considered as process variables.

2. Methodology and experimental

2.1. Materials and electrochemical methods

Austenitic stainless steels are extensively employed in a broad range of applications due to their relatively low cost and good corrosion resistance. Of the 300 series, 316SS is the most widely adopted for fuel cell applications and the focus of this investigation. Coupons ($25 \times 25 \times 0.5$ mm) of 316SS were cut from sheets of $300 \times 300 \times 0.5$ mm (Goodfellow, UK). The wt% chemical composition, as detailed by Goodfellow, is: Cr (16.87%), Ni (10%), C (190 ppm), Mn (1.38%), Si (4600 ppm), P (40 ppm), S (30 ppm) Mo (2.02%) and Fe (balance).

The stainless steel samples to be treated were rinsed with acetone followed by ultra-pure water (18 MΩ, Millipore, UK) and dried by passing warm air over the sample prior to treatment in an electrochemical cell containing solutions of varying ratios of sulphuric acid/glycerol, as described in Table 1.

During the surface modification (electropolishing) process, the coupon samples were immersed at the centre of a cylindrical cell containing 350 ml of electrolyte solution. Temperature control was achieved by a water jacket connected to an isothermal circulated water bath, as seen in Fig. 1. The electrolyte solutions were prepared from analytical grade sulphuric acid 95–97%(EMSURE® ISO, UK) and ultrapure water (18.2 MΩ, Millipore). Viscosity enhancing agent, glycerine/glycerol, 99.5% (Mistral Lab Chemicals, UK) was added to the sulphuric acid at a range of concentrations in order to explore its effects.

The counter electrode was composed of two platinum coated titanium mesh sheets; each with an area of 50×50 mm positioned a distance of 10 mm from the working electrode sample (Fig. 1). A dc current was passed between the sample (working electrode anode) and the counter electrode (cathode) for a range of periods (5, 10, 30 or 60 min). The temperature of all experiments was monitored, with all tests being performed at room temperature (25 ± 0.5 °C) in naturally aerated solutions. The anodisation treatment was conducted via the application of a direct current at 12.5, 25, 50 and 100 mA cm^{-2}, which corresponds to the etching/polishing regime.
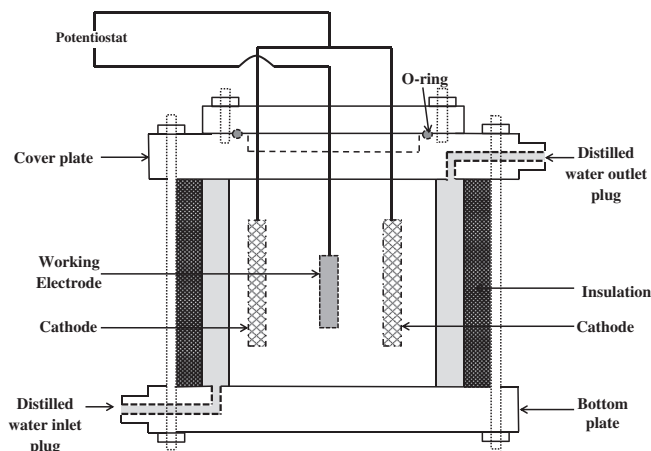
In order to ensure that the corrosion tests carried out on the specimens simulated the aggressive conditions experienced within a PEFC (possible direct contact with electrolyte membrane) and acted as an accelerated test environment, all electrochemical experiments were conducted in 1 M H_2SO_4 + 2 ppm F$^-$ ions [28] at 70 °C in the flushed port electrochemical cell shown in Fig. 2. Polarisation experiments to characterise the 316SS electropolishing regimes with respect to electrolyte concentration (0.25, 0.5 and 1 M H_2SO_4) were performed between 0 and 2500 mV$_{RHE}$ in the electrochemical cell at a scan rate of 1 mV s^{-1} at 25 °C.

All electrochemical testing was conducted using potentiodynamic measurements with a three-electrode thermostated cell

Fig. 1. Schematic diagram of cell used for anodisation treatment.

assembly using a potentiostat (PGSTAT302N, Metrohm Autolab, The Netherlands). The reference electrode was a Standard Hydrogen Electrode (SHE) (Gaskatel, Germany) used to eliminate the risk of contamination of the electrolyte with chloride ions.

In order to evaluate the performance of the treated specimens under representative conditions, potentiostatic tests were carried out at 100 mV$_{RHE}$ in hydrogen-saturated solution and at 800 mV$_{RHE}$ in oxygen-saturated solution to simulate conditions at the anode and cathode respectively [5]. Anodic potentiodynamic curves were obtained at a scan rate of 1 mV s^{-1} (-500–1500 mV$_{RHE}$) for the PEFC anode and cathode corrosion studies. In order to simulate the start-up conditions of a fuel cell, linear sweep voltammetry was performed over the range 600–1500 mV$_{RHE}$ in air saturated electrolyte to simulate fuel cell cathode conditions and OCP to 100 mV$_{RHE}$ in H_2 saturated electrolyte to simulate fuel cell anode conditions. The scans were repeated 200 times at a scan rate of 1 mV s^{-1} with a rest period of 5 min at OCP between each scan. In all experiments electrochemical measurements were started 1 h after immersion of the working electrode in the solution when the OCP had reached steady state within the relevant purged environment.

Table 1
Anodisation treatment and electrolyte solution description.

Assignment	Sulphuric acid electrolyte to glycerol, ratio (v/v)
A.T 1	100:0
A.T 2	90:10
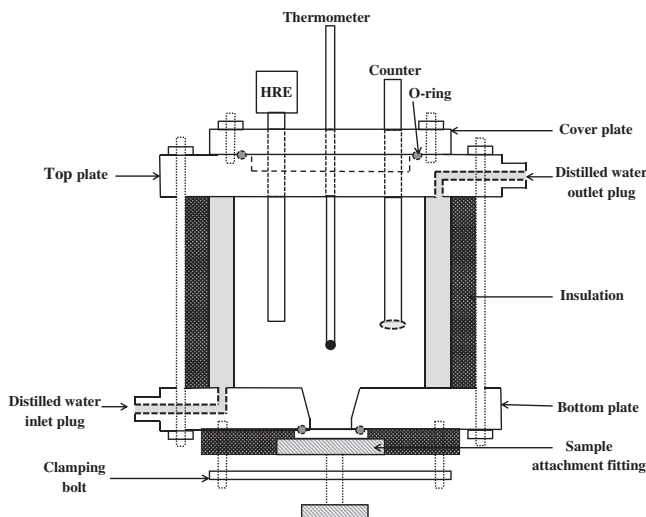
Fig. 2. Schematic diagram of the electrochemical cell used for corrosion studies.
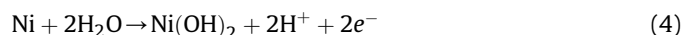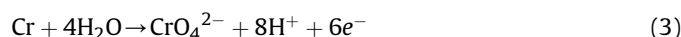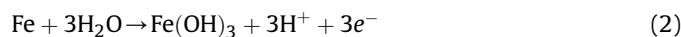
2.2. Current efficiency calculation

A range of additional reactions can occur at the anode during the electrodissolution of stainless steel, including oxygen evolution and chromium reoxidation (following reduction at the cathode). Hydrogen evolution is the primary reaction at the cathode, with side reactions including chromium and sulphate reduction. According to Faraday's law, the current efficiency (η_P) (Equation (1)), can be defined as the ratio between the charge used to form the product (P) and the total charge passed (according to the approach presented by Sánchez-Sánchez et al. [29]).

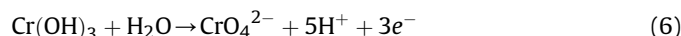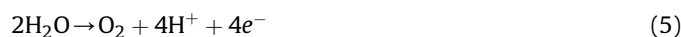$$\eta_P = \frac{\frac{m_P}{M_P}\frac{v_e}{v_P}F}{Q} = \frac{Q_m m_P S}{It} \tag{1}$$

Where: F is Faraday's constant (96,487 C mol^{-1}), m_P is the mass of product, M_P is the molar mass of 316SS in (g mol^{-1}), v_e and v_P are the stoichiometric ratios of electrons and product, Q is the charge passed (coulombs), Q_m is the charge required to electro-dissolve 1 g of 316SS, S is the surface area (cm^2), I is the current (A), and t is the time (s).

The current efficiency calculations are based on the amount of charge required to dissolve 1 g of the stainless steel and assume the highest solution valence state for each metal species (Fe, Cr and Ni) in the calculation. In this case the current efficiency represents the ratio of charge that oxidizes the steel (Equations (2)–(4)) to the total charge that is passed by the reactions in Equations (2)–(6). Once the total mass change is determined by weight loss measurements, the current efficiency is calculated.
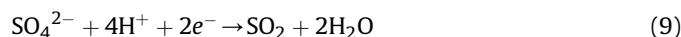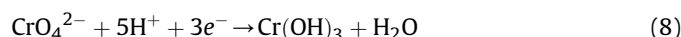
At the anode:

$$Fe + 3H_2O \rightarrow Fe(OH)_3 + 3H^+ + 3e^- \tag{2}$$

$$Cr + 4H_2O \rightarrow CrO_4{}^{2-} + 8H^+ + 6e^- \tag{3}$$

$$Ni + 2H_2O \rightarrow Ni(OH)_2 + 2H^+ + 2e^- \tag{4}$$

With side reactions:

$$2H_2O \rightarrow O_2 + 4H^+ + 4e^- \tag{5}$$

$$Cr(OH)_3 + H_2O \rightarrow CrO_4{}^{2-} + 5H^+ + 3e^- \tag{6}$$

At the cathode:

$$2H^+ + 2e^- \rightarrow H_2 \tag{7}$$

With side reactions:

$$CrO_4{}^{2-} + 5H^+ + 3e^- \rightarrow Cr(OH)_3 + H_2O \tag{8}$$

$$SO_4{}^{2-} + 4H^+ + 2e^- \rightarrow SO_2 + 2H_2O \tag{9}$$

2.3. Interfacial contact resistance

Tests were conducted to establish the relationship between the compaction pressure and contact resistance between the sample and the GDL material. The apparatus shown in Fig. 3 was used to perform this measurement, based on that described by Wang et al. [5] and Davies et al. [13]. The method utilises two pieces of GDL (Toray TGPH090) [5], the materials and compression properties of which have been well characterised by Mason et al. [30] and El-kharouf et al. [31]. This three-layer assembly is then placed between two gold-coated copper plates and a compaction pressure is
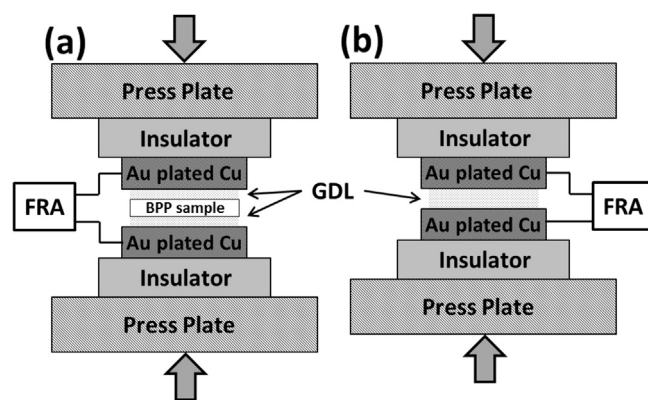

Fig. 3. Illustration of rig used to perform interfacial contact resistance measurements. (Left) arrangement for measuring contact resistance with steel sample, and (Right) arrangement to determine contact resistance between GDL and gold platens.

applied using a hydraulic air ram (series C95SB50-150, SMC, UK) and measured using an integrated load cell (LCM304-2KN, Omega UK).

Electrical resistance measurements were carried out using a potentiostat and a frequency response analyser (PGSTAT302N with FRA2, Metrohm Autolab, The Netherlands) in the frequency range 1–100 kHz with an amplitude of 15 mV. The high frequency intercept with the real axis was chosen to represent the ohmic resistance of the system, which is dominated by the contact resistance between components.

In order to correct for the contact resistance between the GDL and the gold coated copper plates, a calibration in which the two layers of carbon paper are sandwiched between the gold coated copper plates is made. Deducting the calibration from the total contact resistance and halving the results gives the interfacial contact resistance for the carbon paper/BPP interface.

2.4. Surface composition and morphology

Time-of-flight secondary ion mass spectrometry (ToF-SIMS) was carried out using an IONTOF ToF-SIMS V instrument (ION-TOF GmbH, Germany). The mass spectra were collected using a 25 keV Bi$^+$ analytical ion beam in high current bunched mode to obtain high mass resolution. Positive secondary ions were collected, using a primary beam current of $\sim$1 pA (at a 100 μs cycle time). The analytical area was 200 × 200 μm collecting 256 × 256 pixels. Each
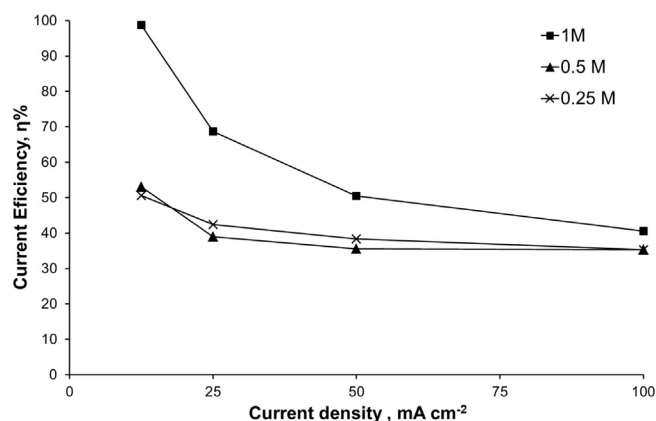

Fig. 4. Current efficiency as a function of current density and H$_2$SO$_4$ concentration at room temperature.
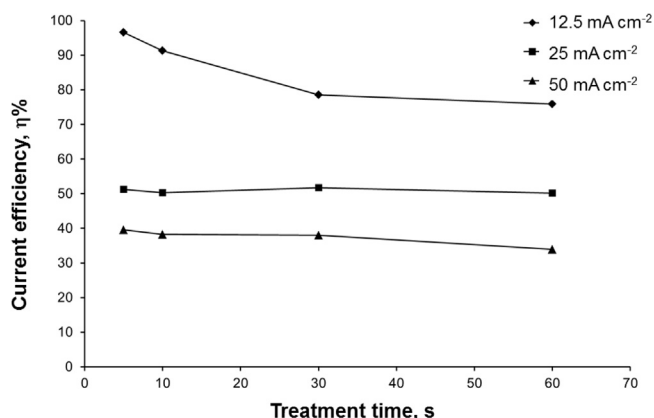
Fig. 5. Current efficiency as a function of treatment time and current density in 0.5 M H$_2$SO$_4$ at room temperature.

analysis was performed with a dose of 5×10^{12} ions cm^{-2}, well within the static SIMS regime.

Scanning electron microscopy (SEM) was conducted using a Zeiss Supra 40 field emission scanning electron microscope at a beam voltage of 15 kV and a scan rate in the range 6.4–25.6 μs. Analysis was made within a scan size of approximately 1.6 mm^2 (400 × 400 μm) at an image magnification of ×900 and ×2500.

Surface morphology was characterized using a Park XE-100 atomic force microscope (AFM) in contact-mode. Imaging of the samples was carried out at 0.75 Hz, with scan sizes of 10, 50 and 90 μm at set point 1.24 nN, providing '3D' rendering with a line scan on each sample and an image of the surface roughness (R_a) for each sample using a NSC14 Cr–Au tip.

3. Results and discussion

3.1. Current efficiency

As shown in Fig. 4, the current efficiency of the anodisation process is dependent on current density and sulphuric acid concentration at ambient temperature (25 °C). The current efficiency

increases with increasing electrolyte concentration and with decreasing current density. The ionic strength of the three sulphuric acid electrolyte solutions (0.25, 0.5 and 1 M) plays a major role in the dissolution rate and consequently on the current efficiency. Higher field strength across the passive layer is associated with higher anion penetration and consequently the amount of metal dissolved. This is because as the oxide matrix is attacked by anions, it exhibits ionic conductivity that results in metal dissolution and thinning of the oxide layer [32]. The effect of ionic strength on current efficiency is further elaborated in work by Hoar et al. [33].

In addition, varying the treatment time at a fixed concentration and current density also demonstrates a decrease in current efficiency with respect to treatment time, as seen in Fig. 5. The electrolysis treatment time is one of two variables in Faraday's law of electrolysis required to determine the total material removed from the sample. As the treatment time increases the amount of material removed from the anode surface increases and consequently the average surface roughness decreases, as demonstrated by Lee [34]. However, the current efficiency is seen to decrease with longer treatment times, most notably at a current density of 12.5 mA cm^{-2} while at 25 and 50 mA cm^{-2} the current efficiency changes are less noticeable over longer treatment times. This is because the rate determining process during electropolishing is one of diffusion of product ions away from the surface; so as the current density increases, mass transport effects become more evident. This rationale is based on the adsorbate acceptor model proposed by Matlosz et al. [35], founded on the concept of acceptor mechanism, which examined the influences of adsorbed intermediates and the transport of acceptor molecules on electropolishing behaviour.

3.2. Process electrochemistry

Fig. 6 shows the polarisation characteristics for the anodisation of 316SS in 0.25, 0.5 and 1 M H$_2$SO$_4$ acid electrolyte at a scan rate of 1 mV s^{-1}. The transpassive region is characterised by an increase in current density associated with the breakdown of the passive film. The onset of a current plateau is observed between ~1450 mV$_{RHE}$ and 1850 mV$_{RHE}$, as typically observed for stainless steels bearing chromium and nickel in acid electrolyte [14,15]. The current plateau in this region is typically associated with the formation of a
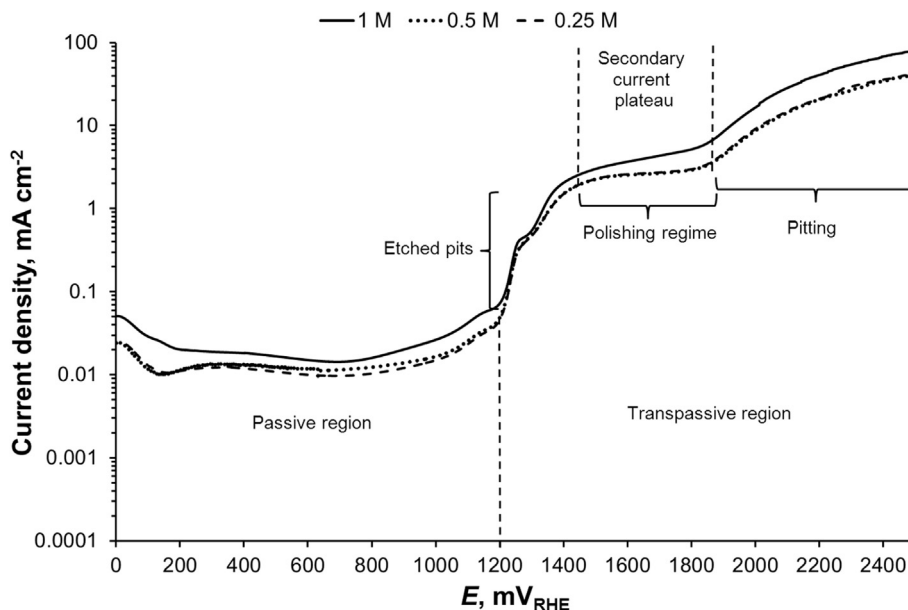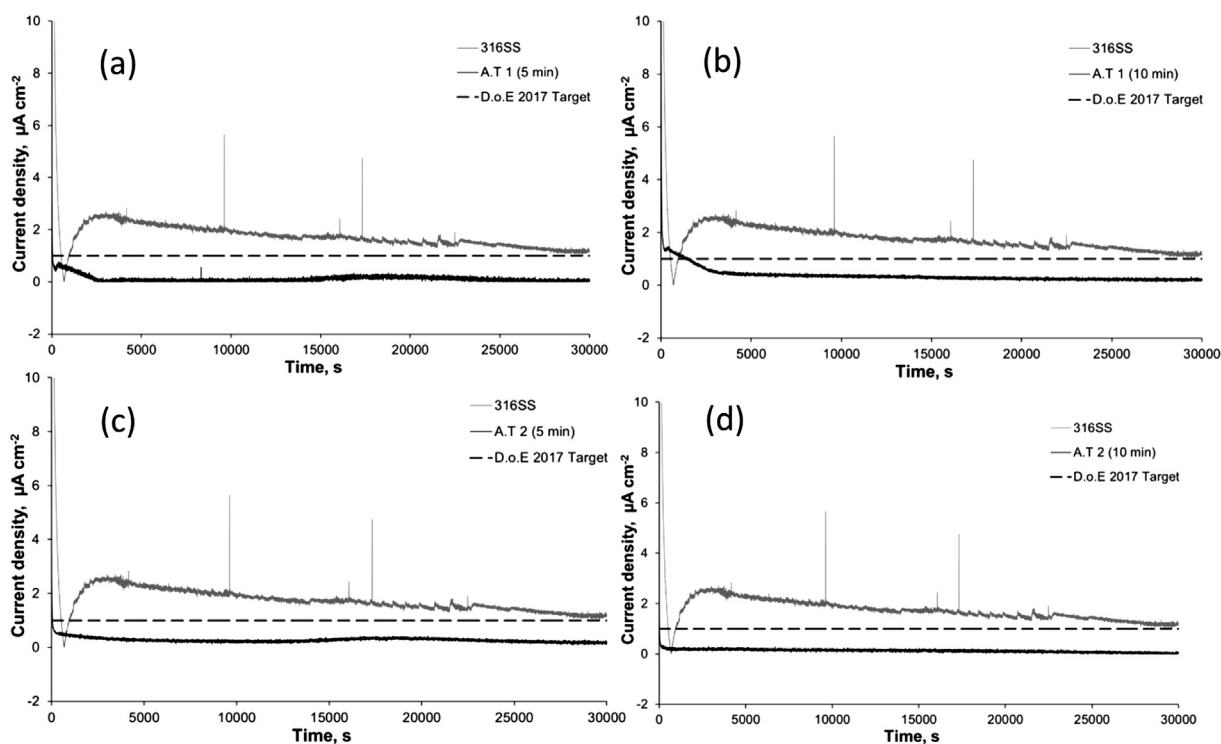

Fig. 6. Polarisation curves (1 mV s^{-1}) obtained on 316SS showing current profile for passive, active and pitting regimes as a function of sulphuric acid concentration.
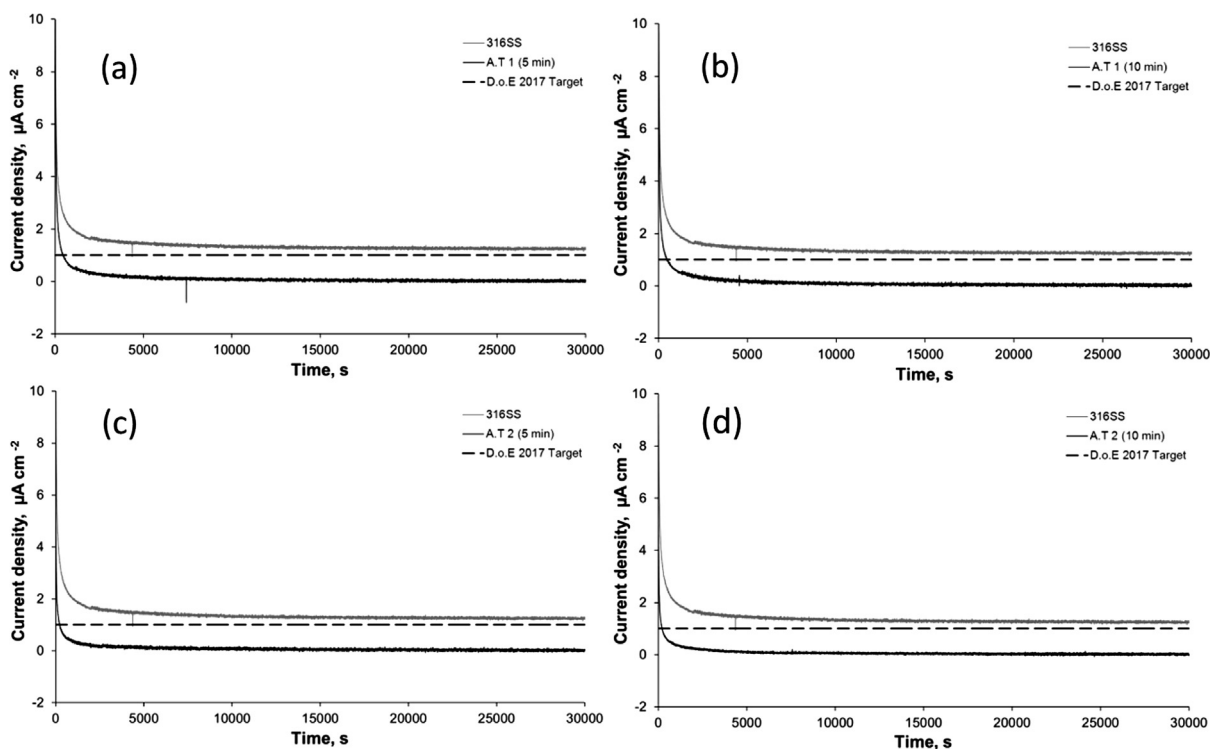
Fig. 7. Current transients for 316SS: (a) A.T 1 (5 min), (b) A.T 1 (10 min), (c) A.T 2 (5 min) and (d) A.T 2 (10 min). Samples at 0.1 V_{RHE} in simulated PEFC anode environment (1 M H_2SO_4 + 2 ppm F^- at 70 °C) purged with H_2.

secondary film which controls the chemical dissolution through its interface with the electrolyte; thereby defining a potential range independent of current [36]. In dilute acid, etching typically occurs in this region at a constant 'limiting' current density. Above

1900 mV_{RHE} oxygen evolution occurs with pitting of the surface of the bulk metal.

As seen in Fig. 6, in 1 M H_2SO_4 electrolyte solution a non-uniform current plateau is observed between 1450 mV_{RHE} and

Fig. 8. Current transients for 316SS: (a) A.T 1 (5 min), (b) A.T 1 (10 min), (c) A.T 2 (5 min) and (d) A.T 2 (10 min). Samples at 0.8 V_{RHE} in simulated PEFC cathode environment (1 M H_2SO_4 + 2 ppm F^- at 70 °C) purged with air.

1850 mV$_{RHE}$, while in 0.5 M and 0.25 M H$_2$SO$_4$ a more uniform etching/polishing current plateau is observed in the same region at lower current densities. The uniform current plateau is ascribed to a quasi-passivation process whereby oxidation leads to an insoluble layer at the electrode surface. In this region the electrode undergoes a transpassive dissolution process that is transport controlled in aqueous solution [37]. On account of the high current efficiency and uniformity in the current density plateau in the polishing regime, as well as the environmental and economic benefits of utilising a less concentrated solution, 0.5 M H$_2$SO$_4$ was chosen as the electrolyte concentration for subsequent anodisation treatments.

3.3. Corrosion performance

Along with cost and performance, the other key metric that dictates the suitability of PEFC technology for large scale commercialisation is durability. The U.S. Department of Energy (DoE) has set lifetime durability targets for 2015 for PEFCs of 5000 h for transportation power systems and 40,000 h for stationary power systems [38]. Over this period fuel cell performance degradation is expected to be maintained at a minimum. For metallic bipolar plates, current DoE targets specify anodic current densities <1 μA cm^{-2} at 100 mV$_{RHE}$ under H$_2$-purged conditions to simulate the anode environment and at 800 mV$_{RHE}$ under aerated conditions to simulate the cathode environment [38].

Corrosion performance was studied over a period of 30,000 s to give an indication of the durability of the passive film under PEFC anode and cathode operating potentials (Figs. 7 and 8).

The effect of the anodization treatment is to significantly reduce the corrosion current density in comparison to that of untreated steel, bringing it well below the US DoE target in both simulated anode (Fig. 7) and cathode (Fig. 8) environments. As noted by Wang et al. [39], the degree of protection offered by the passive film is indicated by the rate of formation over the entire surface. In the anode environment, hydrogen induces passive film dissolution and the length of time required for stable film formation is generally longer than that under fuel cell cathode conditions.
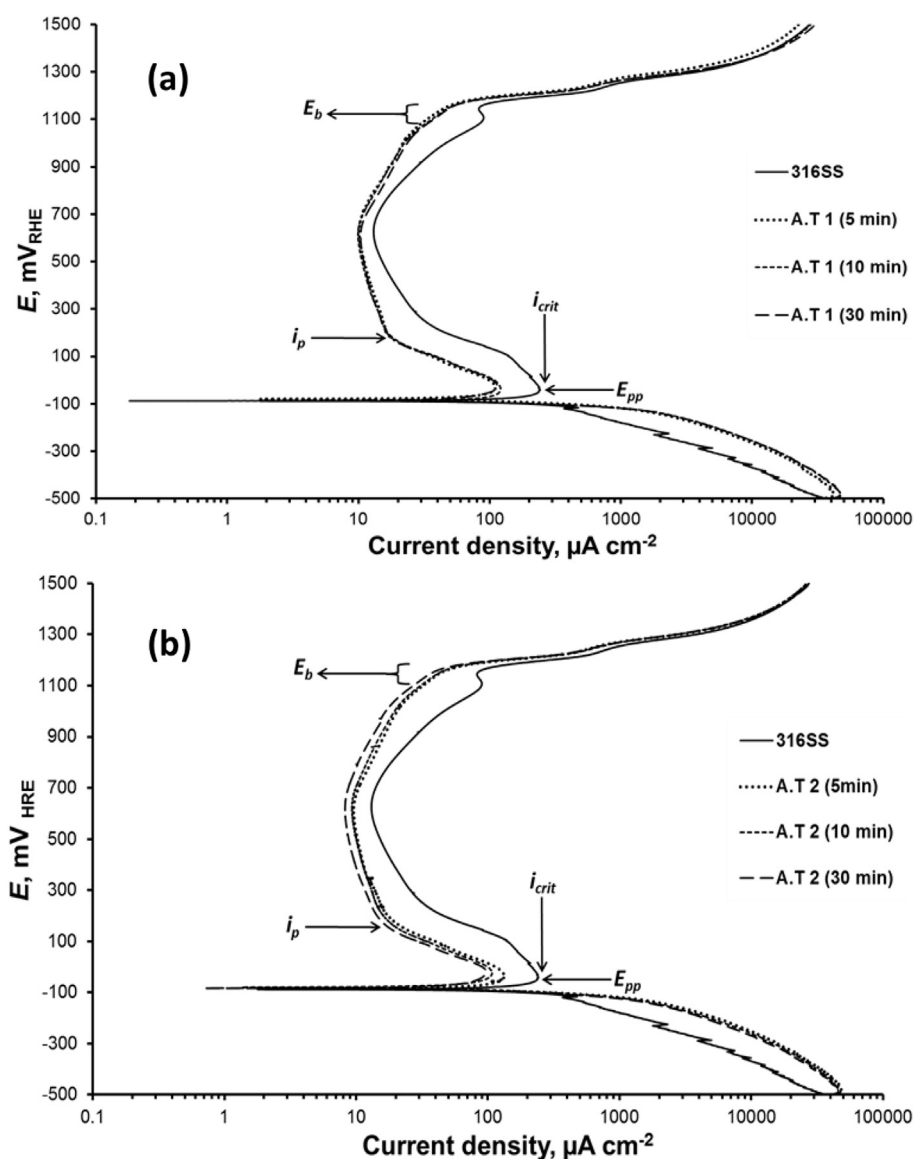

Fig. 9. Polarisation curves of (a) A.T 1 and (b) A.T 2 samples in comparison with untreated 316SS in simulated PEFC anode environment (1 M H$_2$SO$_4$ + 2 ppm F$^-$ ions at 70 °C) saturated with H$_2$.

Rapid transitions to a stable current density can be observed with a greater degree of stability associated with the oxidising environment under fuel cell cathode conditions. The untreated 316SS demonstrated a transient current density of ~ 1.7 μA cm^{-2}, which is above the US DoE target in agreement with Yang et al. [40].

As seen in Figs. 7 and 8, the current stabilization for the samples takes longer in the anode environment than in the cathode environment, more noticeably for the untreated 316SS sample. The longer stabilisation time at the anode is due to the different applied potential, but there may also be a contribution from the absence of O_2 in the electrolyte solution, of which a critical amount is necessary to prevent corrosion by passivating the surface [41].

The polarisation response for two treatment conditions (A.T 1 and A.T 2) in simulated PEFC anode and cathode environments is shown in Figs. 9 and 10 respectively, along with untreated 316SS for comparison.

The potential range experienced by a bipolar plate in contact with a fuel cell anode ($0-100$ mV_{RHE}) coincides with that spanning the active/passive transition for 316SS in an acidic environment. When characterising the corrosion resistance of a material in this region the two key performance parameters are the potential of the active peak (here between -100 and 100 mV_{RHE}) referred to as the critical passivation potential (E_{pp}), and the critical passivation current density (i_{crit}) which gives a measure of the ease of passivation; the smaller the current, the easier the passivation process. As seen in Figs. 9 and 10, the treated samples have significantly lower i_{crit} and a more negative E_{pp}. The active peaks within the anodic dissolution range are also narrower for the treated sample in comparison to the standard 316SS untreated sample. Additionally, the treated samples also demonstrate lower passive current density (i_p) which provides a measure of the protectiveness of the film. This trend is observed for all the treated samples (Figs. 9–12).

In the simulated PEFC cathode environment, the breakdown of the oxide by anions via the initiation of pitting, which occurs at a critical potential called the critical breakdown or pitting potential (E_b) of the passivation process, is the key parameter (observed here between 1000 and 1200 mV_{RHE}). The treated samples (Figs. 11 and 12) all demonstrate more positive pitting potentials compared to untreated 316SS. This is due to a greater resistance to localised breakdown of the passivating oxide film by anions (particularly fluoride ions).
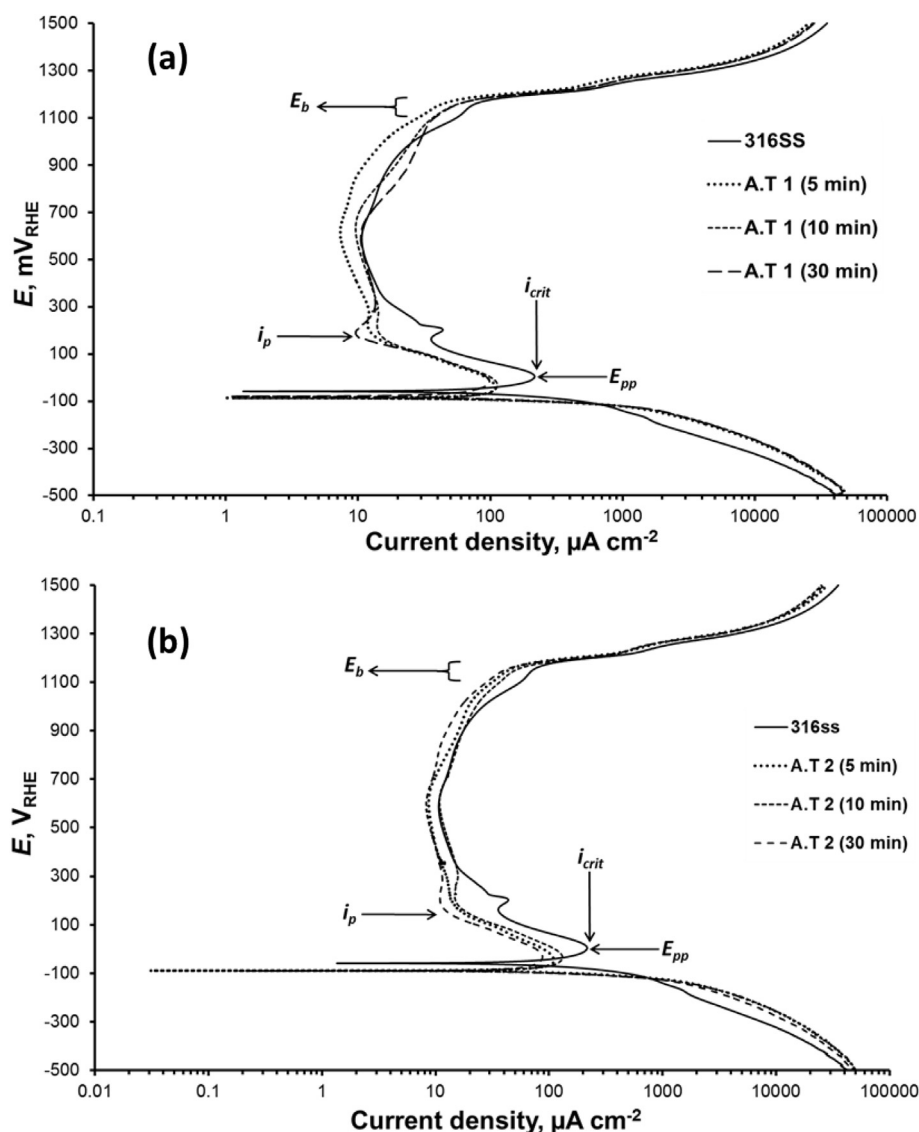
Fig. 10. Polarisation curves of (a) A.T 1 and (b) A.T 2 samples in comparison with untreated 316SS in simulated PEFC cathode environment (1 M H_2SO_4 + 2 ppm F^- ions at 70 °C) saturated with air.
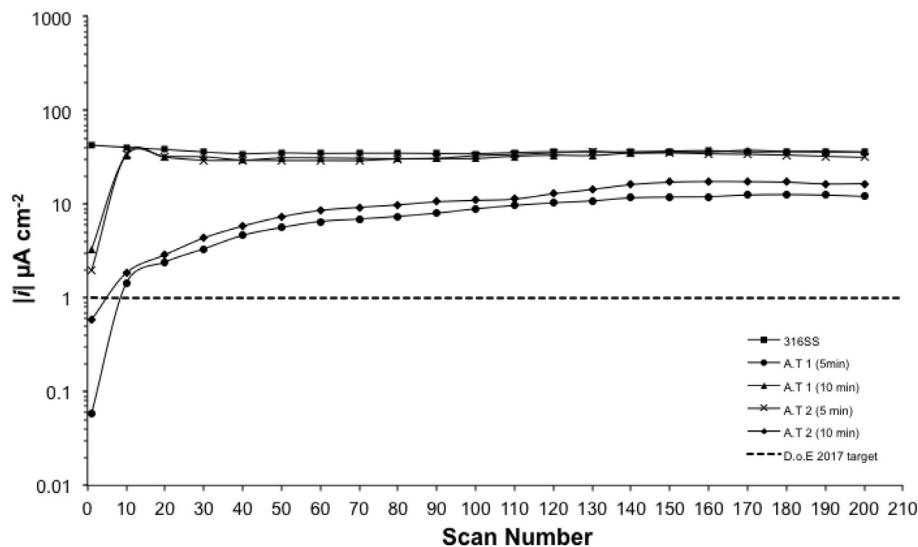
Fig. 11. Current density values over 200 scans (scan rate of 1 mV s^{-1}) at PEFC anode operating potentials (0.1 V); cyclic scans between 0 and 100 mV$_{RHE}$ in fuel cell simulated conditions (1 M H$_2$SO$_4$ + 2 ppm F$^-$ ions), at 70 °C saturated with H$_2$.

These anions induce localised dissolution of the passivating oxide film at 'weak' points, usually associated with discontinuities such as a grain boundaries, dislocations or inclusions in the metal. Similar results for 304SS in sulphuric acid solutions were obtained by Hermas et al. [42].

In order to get an understanding of how the treated samples are likely to perform over extended operating periods, accelerated testing is necessary. Conditions during fuel cell start-up and shutdown can lead to harsher operating conditions with electrode potentials capable of rising to over 1.5 V, as reported by Baumgartner et al. [43].

At the cathode, the high potentials can accelerate pitting corrosion, while at the anode, the low potentials bring about concerns over film stability. The corrosion behaviour of the anodised samples in 1 M H$_2$SO$_4$ + 2 ppm F$^-$ ions, at 70 °C in the fuel anode and cathode operating potential range is shown in Figs. 11 and 12 respectively. The fuel cell anode region is taken to be between

0 and 100 mV$_{RHE}$ to represent the relatively low overpotential of the hydrogen oxidation reaction. The cathode potential range is taken between 600 and 1500 mV$_{RHE}$ to simulate the relatively large overpotential of the oxygen reduction reaction and the possibility of high voltages induced during start/stop processes [43]. On the anode side, all treated samples show initial (~10 scans) current lower than that of untreated 316SS. However, only A.T 1 (5 min) and A.T 2 (10 min) samples show an initial current density below the US DoE's recommended target of 1 μA cm^{-2}, followed by an incremental rise in current densities up to approximately 10 μA cm^{-2} (which is lower than the previous US DoE target of 16 μA cm^{-2}). While both A.T 1 (10 min) and A.T 2 (5 min) demonstrated initial current densities above the U.S DoE's target (~3—4 μA cm^{-2}), with a rapid rise in current densities after 10 cyclic scan to an equilibrating point of ~45 μA cm^{-2}, similar to that of untreated 316SS.

On the cathode side, all the treated samples demonstrated current densities lower that the recommended U.S DoE target
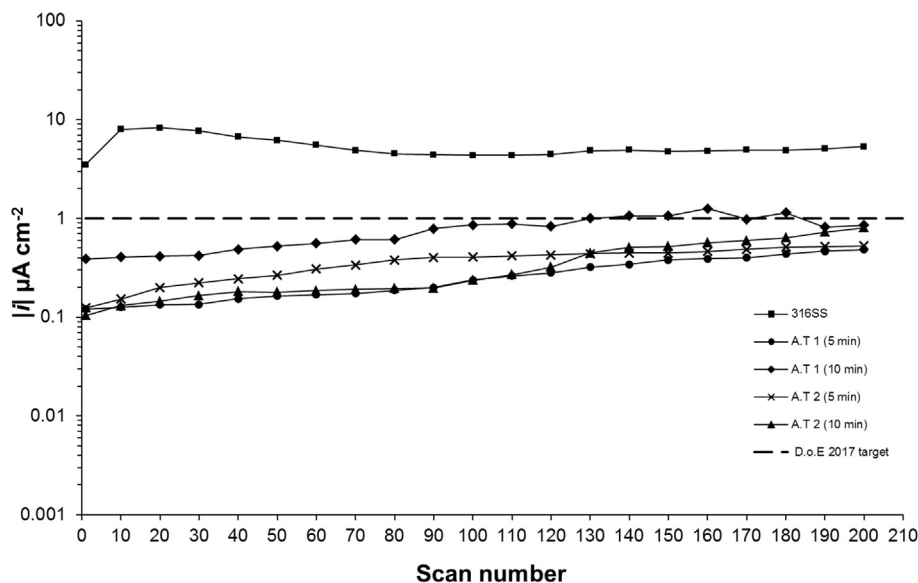
Fig. 12. Current density values over 200 scans (scan rate of 1 mV s^{-1}) at PEFC cathode operating potentials (0.8 V): cyclic scans between 600 and 1500 mV$_{RHE}$ in fuel cell simulated conditions (1 M H$_2$SO$_4$ + 2 ppm F$^-$ ions), at 70 °C saturated with air.
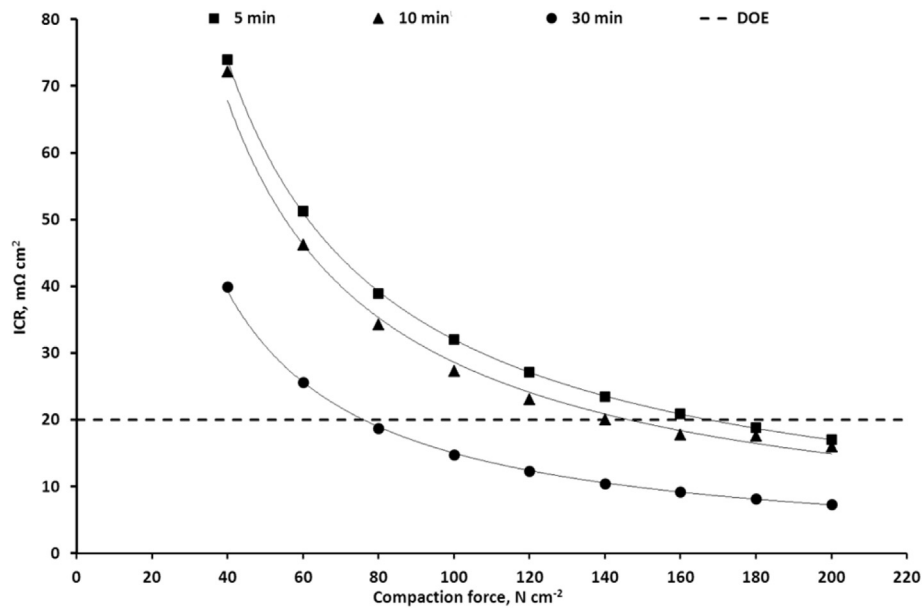
Fig. 13. ICR as a function of compaction force for electrochemically treated 316SS with 0% glycerol additive (A.T 1) at varying treatment times.

initially with a steady increase in current density within the range $0.1–1$ $\mu A\ cm^{-2}$. A.T 1 (10 min) is the only one that demonstrated current densities above the 1 $\mu A\ cm^{-2}$ target after 130 cyclic scans with varied fluctuations beyond this point. The higher current densities observed on the anode side are again attributed to the absence of O_2 in the electrolyte solution, of which a critical amount is necessary to prevent corrosion by passivating the surface [41].

3.4. Interfacial contact resistance

Figs. 13–15 show the relationship between ICR and compaction force ($40–200$ $N\ cm^{-2}$) of the treated samples A.T 1 and A.T 2 in comparison with untreated 316SS. For all samples the ICR decreases monotonically with increasing compression. This trend and the

absolute values for untreated 316SS are similar to those reported by Wang et al. [5]. The electrochemically treated samples demonstrate a common trend of lower ICR values compared to the untreated sample across the whole compaction force range for all treatment regimes. The degree of improvement of ICR is seen to be dependent on the treatment regime, the best performance obtained for the longest treatment time (30 min), which is significantly below the US DoE target of 20 $m\Omega\ cm^2$ at ~140 $N\ cm^{-2}$.

3.5. Surface analysis

3.5.1. Chemical composition

ToF-SIMS was used to study the near-surface chemical compositions of the samples. The near-surface composition has a significant
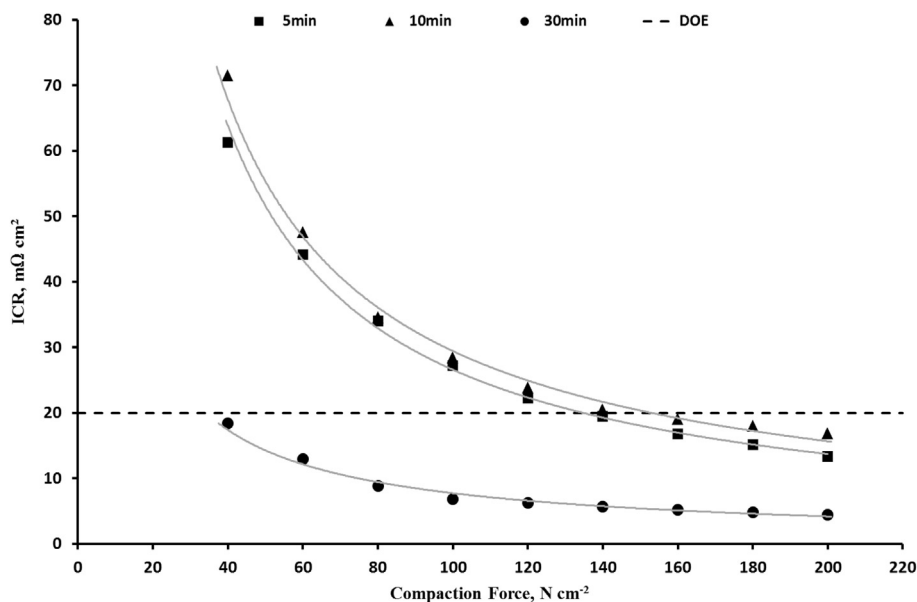

Fig. 14. ICR as a function of compaction force for electrochemically treated 316SS with 10% glycerol additive (A.T 2) at varying treatment times.
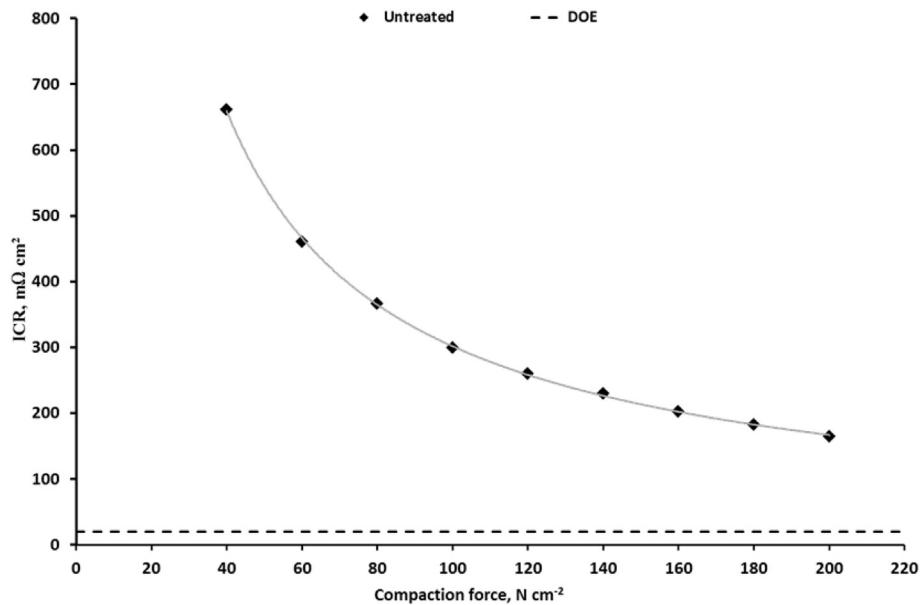
Fig. 15. ICR as a function of compaction force for 316SS.

effect on the properties of stainless steel, as surface oxides can have conducting, semi-conducting or insulating properties depending on the stoichiometric composition. This may have a significant effect on the ICR, with decrease in conductivity due to oxides generally considered to follow the trend of: Ni-oxide > Cr-oxide > Fe-oxide [44]. During the ToF-SIMS analysis not all isotopes for the respective elements could be measured due to mass interferences and poor ion yields. The percentages of the isotopes selected and counted were: Cr 97.3%, Fe 97.6%, Ni 71.7% and Mo 54.8%. The counts were then normalised to 100%, i.e. Cr = Counts/97.3%.

Fig. 16 shows the Fe, Cr, Ni and Mo compositions at the near-surface of the untreated 316SS, compared to the various treated samples. It can be seen that the electrochemical treatment leads to an enhancement in the near-surface content of Cr and Ni, while

reducing the Fe content significantly and the Mo content slightly in comparison to the untreated 316SS sample.

Since the bulk resistivity of stainless steel is insignificant with respect to the surface resistance imparted by the passive film, the chemical composition of the passive film will determine the effective electrical conductivity of the stainless steel. There is a general trend whereby the interfacial resistivity of stainless steel alloys decreases with increasing Ni and Cr content, as demonstrated by Davies et al. [13].

Increased Mo content of stainless steel has been demonstrated to lead to a decrease in the anodic peak by an order of magnitude [36], and has been considered to be a decisive factor in determining contact resistance with greater Mo content demonstrating much lower ICR [45]. The slight reduction in the Mo content between
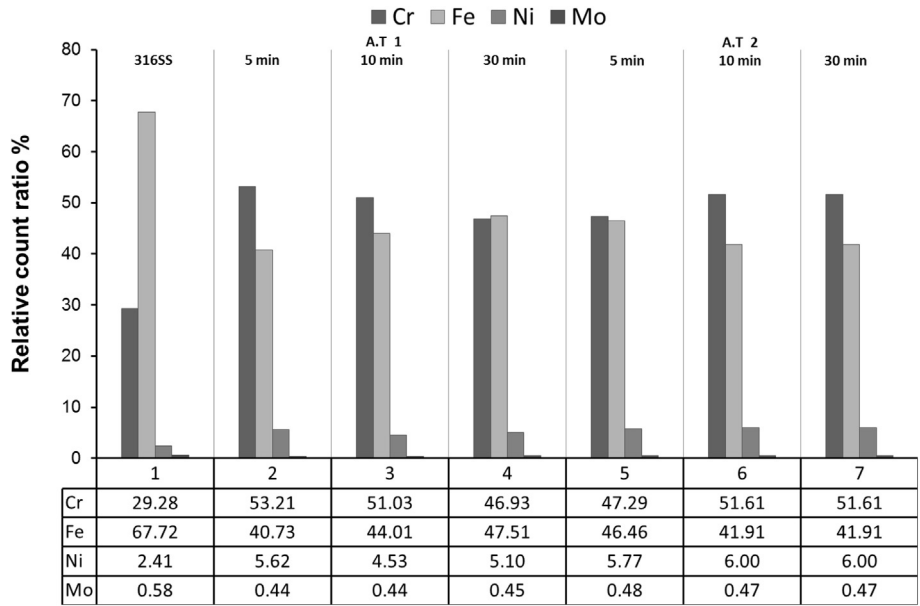

Fig. 16. ToF SIMS isotope count (Fe, Cr, Ni and Mo) of untreated 316SS (1) and treated samples (2—7). See Table 1 for key to sample treatment conditions.
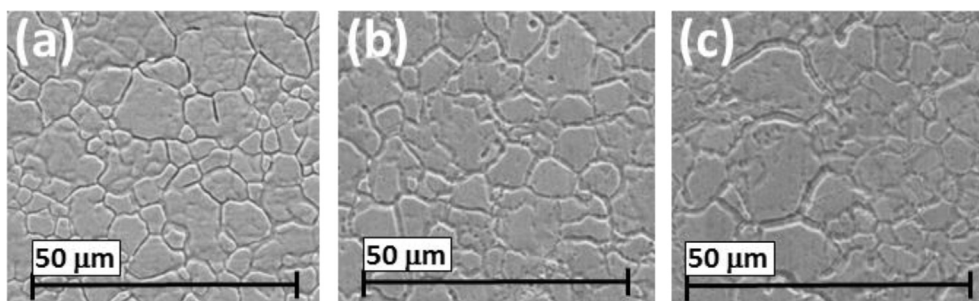
Fig. 17. SEM surface analysis of: (a) untreated 316SS, (b) A.T 1 (5 min), (c) A.T 1 (10 min).

untreated and treated samples implies that Mo is not the reason for improved corrosion resistance and ICR observed here.

As seen in Fig. 16, the relative count ratios for all treated samples lay within a limited range: Cr 46–54%, Fe 41–48%, Ni 4.5–6% and Mo 0.44–0.47%, with minimal changes seen with increases in treatment time and glycerol content. This suggests that shorter treatment times (~5 min) are sufficient to achieve the required surface modification and beyond this the effect of treatment time is minimal.

The presence of glycerol in the electrolyte has an effect on the way the near-surface is modified with time. In the absence of glycerol, extended treatment time actually reduces the Cr content relative to Fe, following the initial significant increase. However, in the presence of glycerol (A.T 2) the Cr/Fe ratio continues to increase with time. The presence of a viscosity modifier is expected to have a hindering effect on the diffusion of metal ions (hydrated metal ions or complex ones) away from the electrode surface. This is due to the fact that glycerol is a relatively large molecule (three OH groups, leading to strong hydrogen bonding between each other) which may be concentrated to form a polymeric structure or aggregates on the surface acting as a shielding layer [46]. This viscous layer formed near the electrode surface controls the rate of dissolution of the anode by controlling the rate at which the products of anodic dissolution can diffuse away; thus the continued increase in Cr/Fe ratio with time in the glycerol containing electrolyte could be used as a means of controlling the process.

3.5.2. Surface topography

Fig. 17 shows the SEM images of untreated 316SS along with the treated samples A.T 1 (5 and 10 min). All of the treated samples exhibited general dissolution over the entire surface, which was associated with surface etching, the effect being more visible along the grain boundaries and with pitting occasionally observed. The dissolution effect along the grain boundary appears to be more noticeable with longer treatment times as the grain boundaries become more prominent. This is because the oxides at the grain boundary are less ordered and therefore more easily dissolved than the more ordered regions within the grains of the metal [33].

The contact area between a BPP and the GDL has a significant effect on the contact resistance and may therefore be correlated to the topography of the BPP. Polished surfaces typically exhibit higher ICR values as they have fewer irregularities, which lowers the density of the contact points between the metal and the carbon fibres [47]. It has been proposed that optimising the surface roughness of the BPP within a suitable range (depending on the GDL structure) can decrease the ICR [47].

AFM measurements were performed to give a quantitative measure of surface roughness. Table 2 compares the ICR at $140 \, \text{N} \, \text{cm}^{-2}$ with respect to the surface roughness parameter (R_a). It is clear that the treatment does not lead to a significant change in surface roughness and therefore morphological change is not attributed to the significant improvement in ICR. Rather, it is the change in near-surface composition, as described in Section 3.5.1, that is the key factor, as suggested by Bai et al. [48]. Lee et al. also suggested improvement of ICR following electrochemical surface treatment of BPP can be attributed to the minimization of the formation of a thick oxide layer that increases ICR [9,18].

4. Conclusions

An electrochemical procedure has been developed with the aim of improving corrosion and contact resistance properties of 316SS for use as bipolar plates in PEFCs. The electrode undergoes a transpassive dissolution process that is transport controlled in aqueous solution with the dissolution process influenced by viscosity modifiers. Polarization studies, as well as ICR measurements on samples treated under two different process conditions of H_2SO_4-to-glycerol ratio (A.T 1 and A.T 2) and different treatment times, showed improved performance with regards to corrosion resistance, ICR and durability of the passive film, when tested against 316SS. Surface analysis showed the composition at the near-surface was enriched with Cr and Ni following treatment in accordance with the improvement of the corrosion resistance and the formation of a thin passive film. Although the surface roughness and surface morphology have been attributed by others as a cause to reduction in ICR, this was not the case here. The key contributing factor to the low ICR was the nature of the passive film dictated by changes in the near-surface elemental composition.

Results suggest that process conditions allow a 'tuning' of the corrosion and contact resistance properties.

Table 2
ICR (at a compaction force of $140 \, \text{N} \, \text{cm}^{-2}$) and R_a values for untreated and anodised 316SS samples.

Sample	ICR ($\text{m}\Omega \, \text{cm}^2$)	R_a (nm)
316SS (Reference)	229.2	24.8
A.T 1 (5 min)	23.5	28.1
A.T 1 (10 min)	20.0	25.3
A.T 1 (30 min)	10.4	15.6
A.T 2 (5 min)	20.5	26.0
A.T 2 (10 min)	19.4	27.0
A.T 2 (30 min)	5.7	18.7

References

[1] D.J.L. Brett, N.P. Brandon, Journal of Fuel Cell Science and Technology 4 (2007) 29–44.
[2] H. Tsuchiya, O. Kobayashi, International Journal of Hydrogen Energy 29 (2004) 985–990.
[3] C.A. Reiser, L. Bregoli, T.W. Patterson, J.S. Yi, J.D. Yang, M.L. Perry, T.D. Jarvi, Electrochemical and Solid State Letters 8 (2005) A273–A276.
[4] H.-C. Kuan, C.-C.M. Ma, K.H. Chen, S.-M. Chen, Journal of Power Sources 134 (2004) 7–17.
[5] H. Wang, M.A. Sweikart, J.A. Turner, Journal of Power Sources 115 (2003) 243–251.
[6] A. Kraytsberg, M. Auinat, Y. Ein-Eli, Journal of Power Sources 164 (2007) 697–703.
[7] P. Kopf, E.J. Carlson, J. Sinha, Y. Yang, in: TIAX LLC Cambridge, Massachusetts, 2005.
[8] W.-J. Meng, Yang Li, Swathy Swathirajan, Stephen J. Harris, Gary L. Doll, in: General Motors Corporation, 1995.
[9] S.-J. Lee, C.-H. Huang, J.-J. Lai, Y.-P. Chen, Journal of Power Sources 131 (2004) 162–168.
[10] J.G. Gonzalez-Rodriguez, M.A. Lucio-García, M.E. Nicho, R. Cruz-Silva, M. Casales, E. Valenzuela, Journal of Power Sources 168 (2007) 184–190.
[11] G.Q. Lu, C.Y. Wang, Journal of Power Sources 144 (2005) 141–145.
[12] H. Wang, J.A. Turner, Journal of Power Sources 128 (2004) 193–200.
[13] D.P. Davies, P.L. Adcock, M. Turpin, S.J. Rowen, Journal of Power Sources 86 (2000) 237–242.
[14] D. Landolt, Electrochimica Acta 32 (1987) 1–11.
[15] K.R. Weisbrod, V.L. Trujillo, H.E. Martinez, LANL Report LA-13225-MS, 1997.
[16] T. Hryniewicz, R. Rokicki, K. Rokosz, Corrosion 64 (2008) 660–665.
[17] R. Kirchheim, B. Heine, H. Fischmeister, S. Hofmann, H. Knote, U. Stolz, Corrosion Science 29 (1989) 899–917.
[18] S.-J. Lee, J.-J. Lai, C.-H. Huang, Journal of Power Sources 145 (2005) 362–368.
[19] K.M. Kim, J.H. Park, J.H. Kim, K.Y. Kim, International Journal of Hydrogen Energy 36 (2011) 9926–9935.
[20] G.F.V. Voort, ASM Handbook, ASM International, 2004.
[21] L.J. Durney, Electroplating Engineering Handbook, Springer, 1984.
[22] C. Wagner, Journal of The Electrochemical Society 101 (1954) 225.
[23] C.-C. Lin, C.-C. Hu, T.-C. Lee, Surface and Coatings Technology 204 (2009) 448–454.
[24] W. Ye, Y. Li, F. Wang, Electrochimica Acta 54 (2009) 1339–1349.
[25] M. Neergat, K.R. Weisbrod, Corrosion Science 53 (2011) 3983–3990.
[26] W.J. McTegart, The Electrolytic and Chemical Polishing of Metals, Pergamon Press, London, 1956.
[27] M. Datta, L.F. Vega, L.T. Romankiw, P. Duby, Electrochimica Acta 37 (1992) 2469–2475.
[28] D.P. Wilkinson, H.H. Voss, in: United States, International Patent number 5441819, 1995.
[29] C.M. Sánchez-Sánchez, E. Expósito, J. Solla-Gullón, V. García-García, V. Montiel, A. Aldaz, Journal of Chemical Education 80 (2003) 529.
[30] T.J. Mason, J. Millichamp, T.P. Neville, A. El-kharouf, B.G. Pollet, D.J.L. Brett, Journal of Power Sources 219 (2012) 52–59.
[31] A. El-kharouf, T.J. Mason, D.J.L. Brett, B.G. Pollet, Journal of Power Sources 218 (2012) 393–404.
[32] K.W. Mao, M.A. Laboda, J.P. Hoare, Journal of The Electrochemical Society 119 (1972) 419.
[33] T.P. Hoar, D.C. Mears, G.P. Rothwell, Corrosion Science 5 (1965) 279–289.
[34] E.S. Lee, The International Journal of Advanced Manufacturing Technology 16 (2000) 591–599.
[35] M. Matlosz, S. Magaino, D. Landolt, Journal of The Electrochemical Society 141 (1994) 410–418.
[36] M. Bojinov, I. Betova, R. Raicheff, Journal of Electroanalytical Chemistry 430 (1997) 169–178.
[37] R.D. Grimm, A.C. West, D. Landolt, Journal of The Electrochemical Society 139 (1992) 1622–1629.
[38] D.o.E. U.S., in: Fuel Cells; Fuel Cell Technologies Program Multi-year Research, Development and Demonstration Plan, 2012.
[39] J. Wang, J. Sun, S. Li, Z. Wen, S. Ji, International Journal of Hydrogen Energy 37 (2012) 1140–1144.
[40] Y. Yang, L.-J. Guo, H. Liu, International Journal of Hydrogen Energy 36 (2011) 1654–1663.
[41] B.S. Covino Jr., M. Rosen, T.J. Driscoll, T.C. Murphy, C.R. Molock, Corrosion Science 26 (1986) 95–107.
[42] A.A. Hermas, M.S. Morad, Corrosion Science 50 (2008) 2710–2717.
[43] W.R. Baumgartner, P. Parz, S.D. Fraser, E. Wallnöfer, V. Hacker, Journal of Power Sources 182 (2008) 413–421.
[44] R.F. Silva, R. Franchi, A. Leone, L. Pilloni, A. Masci, A. Pozio, Electrochimica Acta 51 (2006) 3592–3598.
[45] J.S. Kim, W.H.A. Peelen, K. Hemmes, R.C. Makkus, Corrosion Science 44 (2002) 635–655.
[46] C.-C. Lin, C.-C. Hu, Electrochimica Acta 53 (2008) 3356–3363.
[47] J. André, L. Antoni, J.-P. Petit, E. De Vito, A. Montani, International Journal of Hydrogen Energy 34 (2009) 3125–3133.
[48] C.-Y. Bai, M.-D. Ger, M.-S. Wu, International Journal of Hydrogen Energy 34 (2009) 6778–6789.